PCCP

Accepted Manuscript

This is an *Accepted Manuscript*, which has been through the Royal Society of Chemistry peer review process and has been accepted for publication.

Accepted Manuscripts are published online shortly after acceptance, before technical editing, formatting and proof reading. Using this free service, authors can make their results available to the community, in citable form, before we publish the edited article. We will replace this *Accepted Manuscript* with the edited and formatted *Advance Article* as soon as it is available.

You can find more information about *Accepted Manuscripts* in the Information for Authors.

Please note that technical editing may introduce minor changes to the text and/or graphics, which may alter content. The journal's standard Terms & Conditions and the Ethical guidelines still apply. In no event shall the Royal Society of Chemistry be held responsible for any errors or omissions in this *Accepted Manuscript* or any consequences arising from the use of any information it contains.

PCCP

ARTICLE

Band-Gap Engineering by Molecular Mechanical Strain-Induced Giant Tuning of the Luminescence in Colloidal Amorphous Porous Silicon Nanostructures

A. Mughal,[a] J. K. El Demellawi,[a] and Sahraoui Chaieb[a*]

Nano-silicon is a nanostructured material in which quantum or spatial confinement is the origin of the material's luminescence. When nano-silicon is broken into colloidal crystalline nanoparticles, its luminescence can be tuned across the visible spectrum only when the sizes of the nanoparticles, which are obtained via painstaking filtration methods that are difficult to scale up because of low yield, vary. Bright and tunable colloidal amorphous porous silicon nanostructures have not yet been reported. In this letter, we report on a 100-nm modulation in the emission of freestanding colloidal amorphous porous silicon nanostructures via band-gap engineering. The mechanism responsible for this tunable modulation, which is independent of the size of the individual particles and their distribution, is the distortion of the molecular orbitals by a strained silicon-silicon bond angle. This mechanism is also responsible for the amorphous-to-crystalline transformation of silicon.

Introduction

Since its discovery,[1,2] and notwithstanding the mystery shrouding its visible light emission, porous silicon (p-Si), a nanostructured material in which quantum or spatial confinement is the origin of the material's luminescence, has been found to have many applications, such as light harvesting and detection,[3-5] hydrogen generation,[6] novel tissue culture substrates,[7,8] fuel cells and batteries,[9,10] and biosensing.[11] The ability to select and tune the emission wavelength of p-Si without reliance on size selection such as in Si-nanoparticles,[12] which is expensive and difficult to scale, is attractive for various applications such as light harnessing in micro-devices. Quantum confinement, which is a volume effect due to a particle-in-a-box phenomenon,[13,14] and surface effects, due to surface defects, dangling bonds or molecular species, are claimed to be responsible for the electronic and optical properties of p-Si.[15,16] Tuning the emissions remains elusive. When p-Si is broken into colloidal crystalline nanoparticles, the emission can be tuned across the visible spectrum only when the sizes of the nanoparticles, which are obtained via a painstaking filtration method, vary.[12]

Bright tunable colloidal amorphous porous silicon nanostructures however have not been reported before. Here we achieved a 100 nm modulation of the emission of a novel material made of freestanding colloidal amorphous porous silicon nanostructures through local strain induced by a structural transformation. High Resolution Transmission MIcroscopy (HRTEM), Electron Energy Loss Spectroscopy ((EELS), Raman, Photoluminescence as well as UV-Vis were used in this work to characterize this giant modulation and its physical origin. A simple model capturing the amorphous-to-

crystalline transition is used to explain the correlation between the bond-angle deviation and this tuning effect. We note here that while we achieved a blue shift via an oxidation pathway of our nanostructures, oxidation of silicon nanoparticles was responsible for a red shift instead.[13]

Results and Discussion

We fabricated freestanding colloidal photoluminescent amorphous porous silicon nanostructures (ap-SiNsts) in various solvents using an etchant composed of hydrofluoric acid (HF), hydrochloric acid (HCl), and Iron (III) chloride ($FeCl_3$). This solution creates an electroless chemical reaction in which the metal ion oxidant (Fe^{3+}) injects whole into the valence band of the silicon atoms of the substrate which initiate the reactions that stimulate p-Si formation.[17] This reaction creates a highly phololuminescent p-Si film that exhibits a dual layer structure, in which the top layer, composed of nodules (10 μm in diameter and 6.5 μm thick), that was mechanically unstable and a 1 μm thick bottom layer. We removed the nodules of the top layer using ultrasound bath. These nodules were further broken up by an ultrasonic horn. Suspensions of ap-SiNsts dispersed in toluene sediment faster than those dispersed in ethanol due to the difference in viscosity, because ethanol has a lower density. Ultra centrifugation was used to remove the clusters that are larger than 500 nm in size and that would not remain suspended. Product yields were estimated to be approximately 0.4 mg of ap-SiNsts per cm^2 of Si wafer or 10 mg per 10 ml of solvent. The quantum yield of the nanostructures dispersed in toluene was found to be around 50%.

Samples made in toluene and were kept under N_2 atmosphere were able to maintained their emission for more

than one month. Their emission, centred at 600 nm, did not exhibit a shift in emission or a large decrease in intensity over time. However when the dispersion was mixed with hydrogen peroxide (H_2O_2) we noticed a substantial blue shift. Fig. 1 shows the effect of H_2O_2 on the bright emission from these colloidal solutions. (In the figure, the colloidal solutions are exposed to a UV lamp from below.) The hydrogen peroxide was mixed with the colloidal suspension after sonication. No difference was observed when we dispersed the particles by sonication directly in the mixture.

Fig. 1 Colloidal solutions under UV illumination (365 nm) contained in glass vials. The hydrogen peroxide (H_2O_2) concentration increases from left to right.

TEM micrographs showed that the amorphous porous silicon nanostructures were hundreds of nanometers in size. A high-resolution transmission electron microscope (HRTEM) image and an energy dispersive X-ray spectrum of ap-SiNsts are shown in Fig. 2. This indicates that the particles making up the suspensions were composed of highly porous irregularly shaped structures. Selected area diffraction measurements, taken across the surface of various nanostructures, shown in the inset of Fig. 2, indicated that the material is amorphous. This phase transformation was further verified by Raman spectroscopy (Fig. S1 in the supplementary information) and valence band spectra (Fig. S2 in the supplementary information). The Raman spectra exhibit phonon peaks at 150 cm^{-1} and 480 cm^{-1}. The former peak is related to the transverse acoustic (TA) vibrational mode in amorphous Si, whereas the latter peak is associated with the transverse optical (TO) vibration mode. No peak at 520 cm^{-1}, corresponding to crystalline silicon was ever observed. The range disorder can be estimated using the intensity ratio (TA/TO) as well as the full width at half maximum (Γ) of the TO band which is related to the bond-angle deviation.[18,19]
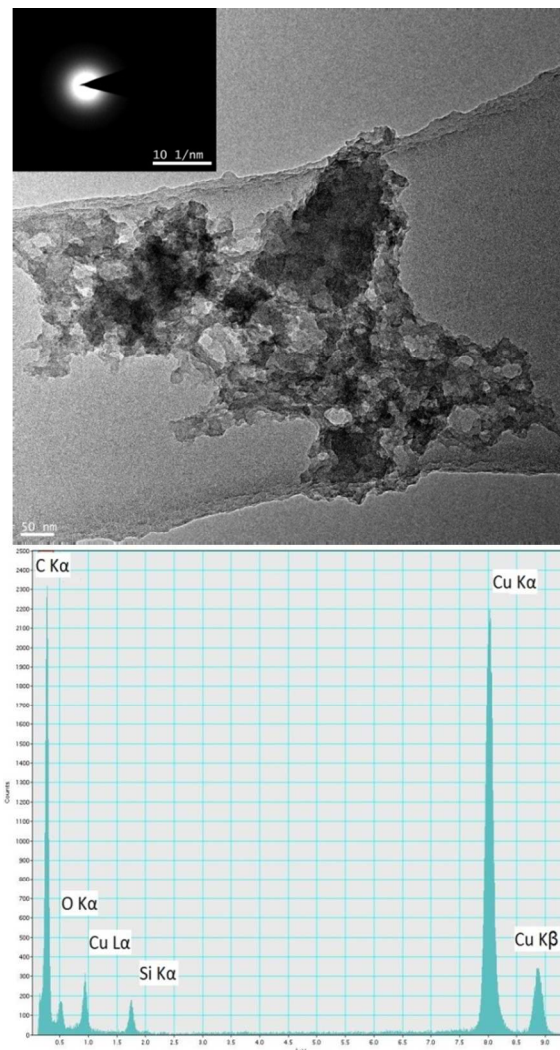
Fig. 2 An HRTEM image of amorphous porous silicon nanostructures (top). The inset is the SAED pattern showing an amorphous structure. EDX (bottom) shows evidence of Si with C and Cu from the TEM grid.

Brunauer-Emmett-Teller (BET) porosimetry measurements indicate that the fabricated nanostructures have an average surface area of 493 m^2/g; similar to activated carbon, with an average pore size of 3.5 nm. This large amount of surface area, which causes the creation of dangling bonds, may be the driving force behind the crystalline-to-amorphous phase transition during the etching process.[20] Gravimetric analysis of the fabricated ap-SiNsts revealed that the average yield was approximately 0.4 mg/cm^2 of etched surface–more than two orders of magnitude greater than what was obtained with crystalline silicon nanoparticles through other etching procedures.

2 | *Phys. Chem. Chem. Phys.*, 2014, **00**, 1-3

This journal is © The Royal Society of Chemistry 2014
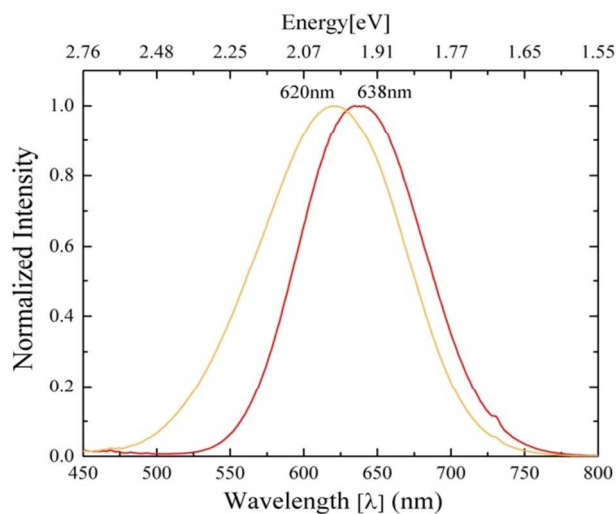
(a)
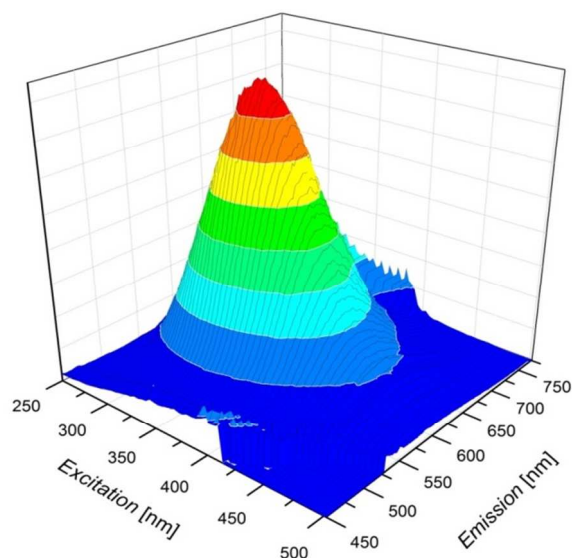
(b)

Fig. 3 (a) PL emission spectra of ap-SiNsts colloidal suspensions (red curve peaking at 638 nm) and the underlying substrate from which it was extracted (orange curve peaking 620 nm). (b) 3D rendering of the PL excitation and emission spectra of ap-SiNsts suspended in Toluene.

As shown in Fig. 3(a), the etched film had an emission peak centered at 620 nm (2 eV) with a full width at half maximum (FWHM) of 0.26 eV, whereas the sonicated films had an emission peak centered at 638 nm (1.94 eV) with an FWHM of 0.3 eV which is narrower than the band of device quality a-Si-H,[21] and much narrower than polysilane alloys (FWHM ~ 0.6-0.7 eV) that emit in the visible range.[22] Fig. 3(b) shows the 3D rendering of the emission and excitation when the nanostructures are suspended in toluene. It is remarkable that the colloidal nanostructures in the suspension, regardless of their size, produce homogenous emissions. The mirror symmetry of the excitation and emission is reminiscent of molecular systems. The photoluminescence emission spectra of the colloidal suspension of the ap-SiNsts as a function of the amount of hydrogen peroxide added to the solvent are shown in Fig. 4.
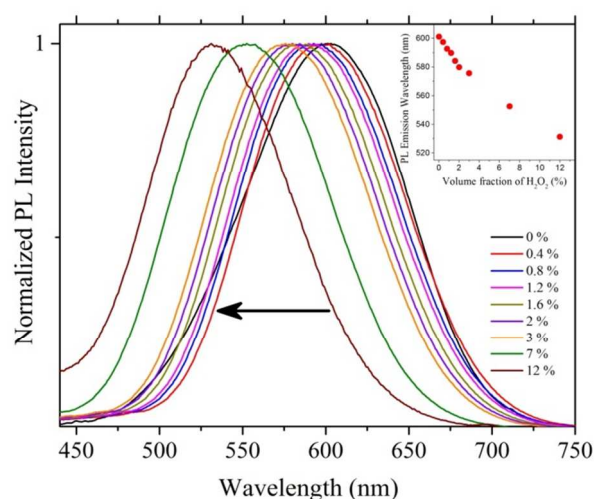
Fig. 4 PL emission spectra of ap-SiNsts colloidal suspensions as a function of the volume fraction of the added peroxide. Notice the blue shift when more peroxide is added. At 12% the fluorescence is weaker as indicated by the noisy fluorescence spectra. The inset shows the maximum emission wavelength versus the added hydrogen peroxide volume fractions typically from 0.4% to 12%.

An X-ray photoelectron spectroscopy (XPS) survey scan of the ap-SiNsts surface as well as the detailed fitting of the Si_{2p} region (Figure S3 in the supplementary information) shows that Si and O are the primary elements detected, with only traces of C present on the surface. H is beyond the detection limits of this analysis technique. Fourier transformed infrared (FT-IR) analysis was performed to determine the relationship between the surface species and emission wavelengths and the degree of oxidation. The corresponding FT-IR absorbance spectra (Figure S4 in the supplementary information) show that the blue-shift in the emission spectra is related to the creation of a new species of silicon oxide (SiO_2) in the bulk as well, which is also supported by EELS data presented below.

The infrared (IR) bands at 3630 cm^{-1} that appears from silicon oxide can be further confirmed by the absorption data in conjunction with the scanning transmission electron microscope (STEM). Samples were examined by spatially resolved energy-loss spectroscopy in STEM. The silicon $L_{2,3}$ absorption edge was measured in the 85-130 eV loss region, where the shape of the silicon is edge related to the chemical bonding, oxidation state and degree of disorder of the material.

This journal is © The Royal Society of Chemistry 2014

Phys. Chem. Chem. Phys., 2014, **00**, 1-3 | **3**
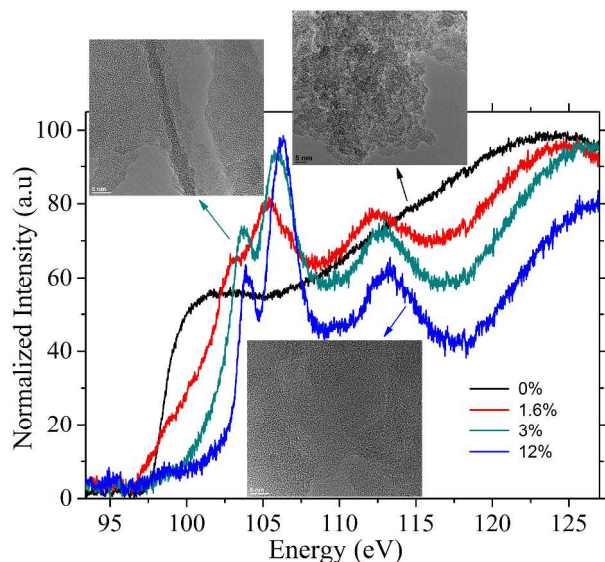
Fig. 5 Si $L_{2,3}$ absorption edge of amorphous silicon nanostructured particles with various oxidation states. The colors correspond to the same amount of peroxide added. Notice the new silicon oxide peak around 105 eV. The Black curves correspond to unoxidized ap-SiNsts. They appear to be silicon.

Fig. 5 shows the Si $L_{2,3}$ edge recorded from an ap-SiNsts sample as a function of its oxidation where it is clear that the $L_{2,3}$ absorption edge increases in energy as the oxidation increases. The spectrum in black is typical for non-oxidised ap-SiNsts. The other spectra are easily distinguishable from the spectrum of the native amorphous nanostructured particles (non-oxidised), forming a fingerprint that compares them from it. Because our samples were relatively thick, multiple scatterings could shift the spectra to higher energies without affecting their structure.[23] In Figure 5, we see the appearance of a peak at 104 eV typical of quartz. The edge spectrum for non-oxidised amorphous p-Si nanoparticles "takes off" around 98 eV but the oxidised ones have a tail and a peak at 104 eV. This shift is due to the difference in the band-gap, which is also clear from the UV-Vis absorption spectra shown in Fig. S5 (supplementary information). The flatness of the spectra until 104 eV and the appearance of the peak at 113 eV are also a signature for silicon oxide and have been attributed to αquartz.[24] The oxidation not only changed the emission spectra but the overall structure of the particles. Fig. S5 (supplementary information) shows how the absorbance drastically changes when peroxide is added to the dispersion. A dramatic structural change is clearly noticeable in the TEM images that accompany the spectra, where the structure becomes more like a "glassy" phase with a finer structure when more hydrogen peroxide is added [20].

The modification of the band-gap in nanostructures might result from a structural modification such as confinement but this not always the cases.[25] This modification of the band-gap can occur at the conduction band or the valence band. $L_{2,3}$ absorption spectroscopy measures the excitation of the occupied core shell $p_{3/2,1/2}$ electrons to the empty conduction band. The absorption threshold is related to the conduction band minimum s-like electronic states due to the golden Fermi rule. Keeping in mind that $p_{3/2,1/2}$ energy is given by the number of valence electrons, and that silicon has 4 of them, it is possible to determine the shift in the conduction band by determining the shift in the absorption threshold. For that, we took the derivative of the spectra in Fig. 5 and the results are displayed in Fig. S6 (supplementary information). The doublet peaks are the spin-orbit split ($p_{3/2}$ and $p_{1/2}$) components of the

L-shell electrons. (One alternative method would be to fit the spectra to an arctangent but the baseline is not always clear, making this method difficult to systematise.[26]) The spectrum for non-oxidized particles is a signature of pure silicon with no visible peaks, but when the structure is oxidised, a clear silicon oxide peak is visible. The $p_{3/2}$ peak shifts while the peak at lower energy does not systematically change when the oxidation is increased. It is clear that the oxidation causes the conduction band to shift at higher energies, which correlates well with the blue shift in the emission. XPS measurements are under way to detect the shift in the valence band and hence enable us to measure the change in the band-gap as a whole beyond the optical band-gap measured using UV-Vis and shown below. We now wonder if we can relate this dramatic change of structure to a mechanical origin.

To probe how the structural disorder in the fabricated ap-SiNsts affects the emission spectrum, we measured the TA/TO ratio from the Raman spectra and found that after 1% of peroxide, this ratio drops abruptly to lower values, indicating a strong change in the structure of the ap-SiNsts toward higher disorder as shown in Fig. S7 (supplementary information). A more quantitative and direct measure of the disorder is that of the bond-angle deviation ($\Delta\theta$) from the width of the Raman spectra, which also suggests a tendency of the structure to become more disordered at the same oxidation (Fig. S7 in the supplementary information). So far, this is the best measure of the amount of disorder in colloidal amorphous silicon.[18,20] To relate the optical properties to a structural change, the peak PL energy was plotted versus the bond-angle deviation.

The variations in the photoluminescence peak energy with the bond-angle deviation are shown in Fig. 6, which demonstrates the pronounced blue shift of the photoluminescence (PL) with increased bond-angle deviation. (The two measurements are independent.) Furthermore, at low angles, the data are best fit such that the peak energy (E) behaves like $E \sim K_{\Delta\theta} (\Delta\theta)^2 + E_o$. In this equation, $K_{\Delta\theta}$ is a stiffness proportional to the number of silicon atoms and to the bond-bending force constant of the Keating potential.[27,28] After the angle of 9.7 degrees, the stiffness of the network doubles, mainly due to the densification of the network towards a glassy phase since the bond-bending stiffness would not vary. From the previous fit, the intercept of the linear fit gives $E_o = 1.48$ eV. If we assume that the emission intensity can be approximated by a Boltzmann distribution, which can be written as $I(h\nu) \sim (h\nu - E_g - E_{elastic})^{\frac{1}{2}} exp(-\frac{h\nu - E_g - E_{elastic}}{k_B T})$, then the maximum of this distribution would be at $(h\nu)_{max} \approx (E_g + E_{elastic} + \frac{1}{2} k_B T)$. In the previous equations, $E_{elatsic}$ is the elastic energy stored when the bond angles vary by an amount ($\Delta\theta$) and should be equal to $K_{\Delta\theta} (\Delta\theta)^2$. Since $\frac{1}{2} k_B T \sim 0.0258$ eV, $E_o + \frac{1}{2} k_B T \sim 1.5$ eV, which is surprisingly close to the band-gap of amorphous silicon. (We should keep in mind that our samples are not conventional bulk amorphous silicon.) This dependence of the photoluminescence energy on the square of the bond-angle deviation is puzzling and similar to the harmonic approximation of the spin glass energy for random alloys introduced by Edwards and Anderson.[29] In analogy to spin glasses, the control parameter here is the amount of oxide that affects the topology of the material and the order parameter is the bond-angle deviation that defines the amount of disorder in the system. The reason for the blue shift is the distortion of the p-orbitals when the bond angle varies by an amount larger than 7 degrees. The origin of this critical angle is not yet understood. From this, we can conclude that the elastic deformation is directly responsible for the blue shift. This deformation is probably responsible for distorting the molecular orbitals.

4 | *Phys. Chem. Chem. Phys.*, 2014, **00**, 1-3

This journal is © The Royal Society of Chemistry 2014
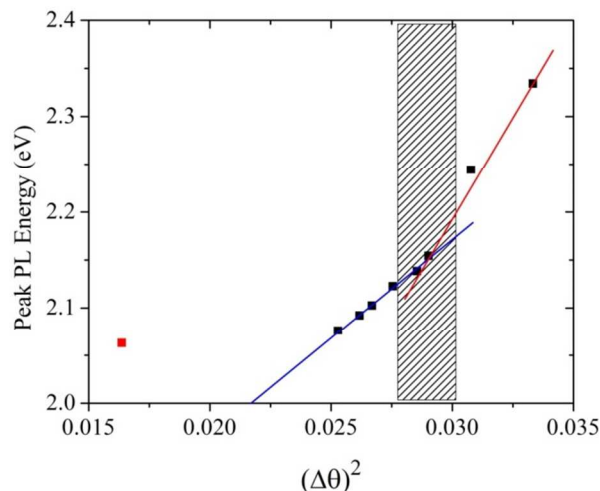
Fig. 6 The PL peak energy as a function of the square of the deviation in the bond angle. The line is a best fit to $K(\Delta\theta)^2$. The shaded box (same region as in Figure 4 in the supplementary information) corresponds to the region where the structure becomes glassy and where the stiffness of the network is doubled. The red square is the energy peak for non-oxidized nanostructured particles.

Optical measurements, such as UV-Vis absorption spectra, can be used to estimate the band-gap energy (E_g) especially in samples like ours that are not heavily doped. Using the bond-angle deviation retrieved from the Raman spectra, we could estimate the dependence of the optical band-gap of these nanoparticles as a function of the oxidation percentage and as a function of the deviation bond angle, $\Delta\theta$. The results are presented in Fig. 8. The fit to the data points correspond to a model where the tetrahedral structure becomes bi-stable when the bond angle increases. This theory will be the subject of a future publication. These results confirm the above results that the band-gap is transformed by a change in the bond angle that distorts the molecular orbitals.
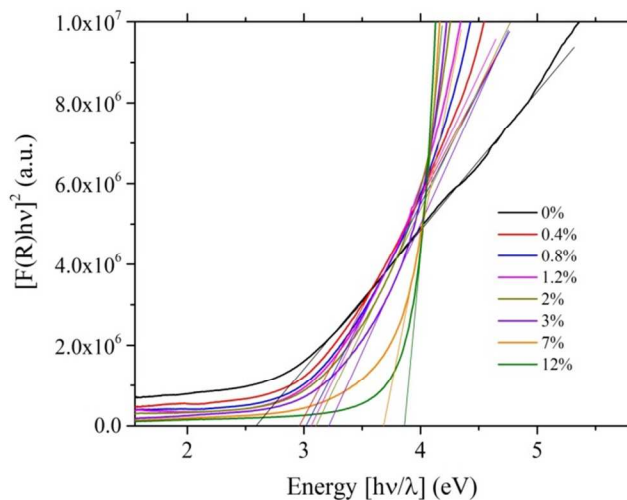
Fig. 7 The optical band-gap at each oxidation state is obtained through linear extrapolation of the Urbach tails of the UV-Vis absorbance spectra.
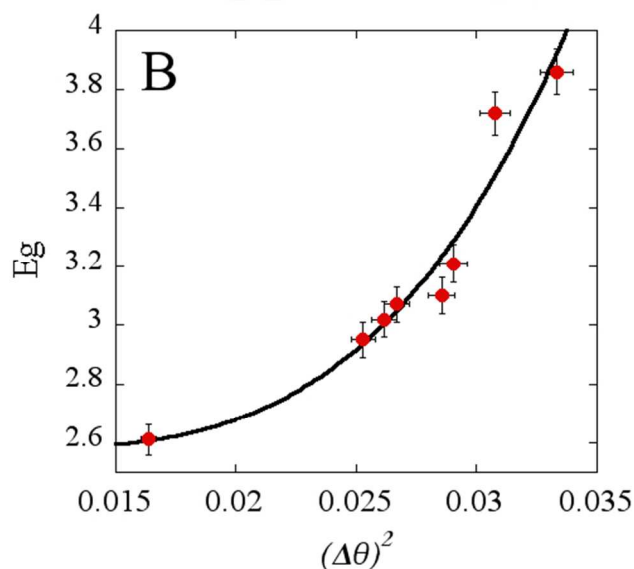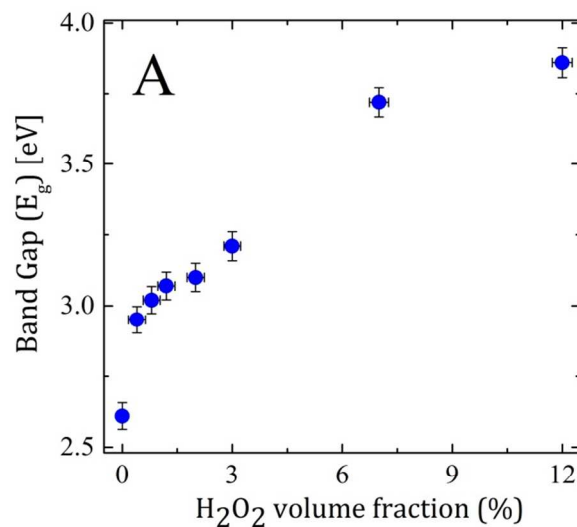
Fig 8. Band gaps are plotted as a function of (A) the percentage of volume fraction of hydrogen peroxide, and (B) the square of the deviation in bond-angle. The fit is of the form of a Landau-Ginzburg expansion.

Experimental Section

Materials Synthesis

Amorphous porous silicon (ap-Si) suspensions were prepared through etching and sonicating single crystal (100) p-type boron doped silicon wafers (Addison Electronics), which were cleaved into 2.5 x 4.5 cm strips. Si strips were submerged in an etching bath composed of 4.7 g anhydrous Iron (III) Chloride (98%, Alfa Aeser) dissolved in a mixture of 18 ml of hydrochloric acid (32%, Fischer Scientific) and 42 ml of hydrofluoric acid (49%, Fluka). Si strips were submerged in the etching bath for 15 hours, after which their surface became matte black. We cleaned the etched strips by rinsing them in deionized water (Millipore) followed by absolute ethanol (Sigma Aldrich). We then dried the strips under a nitrogen stream. After drying, a yellow film formed on the surfacel (Sigma Aldrich). We then dried the strips under a nitrogen stream. After drying, a yellow film formed on the surface.

The etched strips were submerged in a solvent, either ethanol or toluene (Chromasolve grade, Fischer Sci.) and sonicated using a VWR Ultrasonic Cleaner sonicating bath for 30 minutes. Si strips were then removed and the solution containing the ap-Si suspensions were further sonicated using a QSonica Q500 ultrasonic processor for 30 min. Solutions in ethanol were degassed for 20 min using a degassing station (TA Instruments) and sealed under nitrogen. Resulting solutions were a cloudy orange-yellow mixture.

Instrumentation

HRTEM images were recorded on a FEI Krios CT transmission electron microscope at an operating voltage of (120kV). Raman spectra were obtained using a Horiba LabRam ARAMIS Raman spectrometer employing a 473 nm laser beam. Fluorescence spectra were determined on a Horiba Fluoromax-4 Spectrofluorometer. FT-IR spectra were recorded using a Thermo Nicolet iS10 FT-IR spectrometer. Samples were prepared for FT-IR measurements by drying suspensions in KBr salts and pressing them into pellets. XPS characterization was obtained using an Axis Ultra DLD.

Conclusions

We synthesized large quantities of amorphous porous silicon nanostructures that were much brighter than silicon nanocrystals with a quantum yield around 50%. We engineered their band-gap through controlled oxidation that resulted in the deformation of the bond angle. These nanostructured particles emit in the red (~ 620 nm) but their emission is modulated and blue shifted by controlled oxidation, which induces a mechanical deformation of the local structure affecting the position of the conduction band. Current experiments are under way to quantify the shift of the valence band as well. The mechanism of light emission discussed here is probably similar to the spatial confinement discussed by Wehrspohn *et al.*,[30] but we believe that the emission is due to a special case of quantum confinement by structural modification via a glass transition. Since amorphous Si contains localized electronic states, excitons are confined spatially. The nanostructures found in ap-Si cut off these localized excitons from non-radiative recombination centers, thus allowing for the emission of photons. The band-gap of conventionally produced amorphous silicon can range between 1.5 and 2 eV depending on processing conditions.[31] This should result in light emission from wavelengths greater than 620 nm. However, our samples exhibited a blue shift with a band-gap around 3 eV. It is typically assumed that hydrogen forms new bonding states deep within the Si valence bands with little change to the conduction bands, but we demonstrated in this paper that this assumption is not true since we were able to modify the conduction band by removal of hydrogen by oxidation and probably affecting the structure. To our knowledge, this is the first time such a large blue-shift has been observed in colloidal amorphous porous Si and we achieved this by increasing the amount of disorder in the nanostructures of amorphous silicon that exhibit highly uniform emission spectra. These colloidal nanostructures can be used in many applications, such as liquid LEDs, liquid filters and solar energy harvesting as well as oxygen detection in solution and on surfaces.

Acknowledgements

Notes and references

*a*Division of Physical Sciences and Engineering, King Abdullah University of Science and Technology (KAUST), Thuwal, 23955-6900 (KSA).

*E-mail: sahraoui.chaieb@kaust.edu.sa

1   L. T. Canham, *Appl. Phys. Lett.* 1990, **57**, 1046–1048.

2   R. W. Fathauer, T. George, A. Ksendzov and R.P. Vasquez, *Appl. Phys. Lett.* 1992, **60**, 995–997.

3   L. T. Canham, *Nature* 2000, **408**, 411–412.

4   J. P. Zheng, K. L. Jiao, W. P. Shen, W. A. Anderson and H. S. Kwok, *Appl. Phys. Lett.* 1992, **61**, 459–461.

5   F. Ramiro-Manzano, R. Fenollosa, E. Xifré-Pérez, M. Garín and F. Meseguer, *Adv. Mater.* 2011, **23**, 3022–3025.

6   F. Erogbogbo, T. Lin, P. M. Tucciarone, K. M. LaJoie, L. Lai, G. D. Patki, P. N. Prasad and M. T. Swihart, *Nano Lett.* 2013, **13**, 451–456.

7   K. A. Kilian, L. M. H. Lai, A. Magenau, S. Cartland, T. Bocking, N. Di Girolamo, M. Gal, K. Gaus and J. J Gooding, *Nano Lett.* 2009, **9**, 2021–2025.

8   M. Xue, X. Zhong, Z. Shaposhnik, Y. Qu, F. Tamanoi, X. Duan and J. I. Zink, *J. Am. Chem. Soc*. 2011, **133**, 8798–8801.

9   J. Rong, C. Masarapu, J. Ni, Z. Zhang and B. Wei, *ACS Nano* 2010, **4**, 4683–4690.

10 M. Ge, J. Rong, X. Fang and C. Zhou, *Nano Lett.* 2012, **12**, 2318–2323.

11 C. K. Tsang, T. L. Kelly, M. J. Sailor and Y. Y. Li, *ACS Nano* 2012, **6**, 10546–10554.

12 G. Belomoin, J. Therrien, A. Smith, S. Rao, R. Twesten, S. Chaieb, S.; M. H. Nayfeh, L. Wagner and L. Mitas, *App. Phys. Lett.* 2002, **80**, 841–843.

13 M. V. Wolkin, J. Jorne, P. M. Fauchet, G. Allan and C. Delerue, *Phys. Rev. Lett.* 1999, **82**, 197–200.

14 J. Heitmann, F. Müller, M. Zacharias and U. Gösele, *Adv. Mater.* 2005, **17**, 795–803.

15 Y. Kanemitsu, *Phys. Rep.* 1995, **263**, 1–91.

16 A. G. Cullis, L. T. Canham and P. D. Calcott, *J. Appl. Phys.* 1997, **82**, 909–965.

17 M. E. Dudley and K. W. Kolasinski, *Phys. Status Solidi A* 2009, **206**, 1240–1244.

18 D. Beeman, R. Tsu and M. F. Thorpe, *Phys. Rev. B* 1985, **32**, 874–878.

19 R. L. C. Vink, G. T. Barkema and W. F. van der Weg, *Phys. Rev. B* 2001, **63**, 115210-115215.

20 M. M. J. Treacy and K. B. Borisenko, *Science* 2012, **335**, 950–953, PMID: 22363003.

21 R. A. Street, in *Technology and Applications of Amorphous Silicon*, Springer Series in Materials Science **37**; Springer-Verlag, Berlin Heidelberg, 2000, pp 1–6.

22 D. Wolford, B. Scott, J. Reimer and J. Bradley, *Physica B+C* 1983, **117**, Part 2, 920–922.

23 P. Batson, K. Kavanagh, C. Wong and J. Woodall, *Ultramicroscopy* 1987, **22**, 89–101.

24 L. Dori, J. Bruley, D. J. DiMaria, P. E. Batson, J. Tornello and M. Arienzo, *J. Appl. Phys.* 1991, **69**, 2317–2324.

25 D. J. Lockwood, Z. H. Lu and J.-M. Baribeau, *Phys. Rev. Lett.* 1996, **76**, 539–541.

26 J. R. I. Lee, R. W. Meulenberg, K. M. Hanif, H. Mattoussi, J. E. Klepeis, L. J. Terminello and T. van Buuren, *Phys. Rev. Lett.* 2007, **98**, 146803–146806.

27 P. N. Keating, *Phys. Rev.* 1966, **145**, 637–645.

28 P. Roura, J. Farjas and P. R. I. Cabarrocas, *J. Appl. Phys.* 2008, **104**, 073521–073528.

29 S. F. Edwards and P. W. Anderson, *J. Phys. F: Met. Phys.* 1975, **5**, 965–974.

30 R. B. Wehrspohn, J.-N. Chazalviel, F. Ozanam and I. Solomon, *Eur. Phys. J. B* 1999, **8**, 179–193.

31 W. Futako, T. Kamiya, C. M. Fortmann and I. Shimizu, *J. Non-Cryst. Solids* 2000, **266-269**, Part 1, 630–634.

32 M. H. Brodsky, M. Cardona and J. J. Cuomo, *Phys. Rev. B* 1977, **16**, 3556–3571.

33 G. Lucovsky, J. Yang, S. S. Chao, J. E. Tyler and W. Czubatyj, *Phys. Rev. B* 1983, **28**, 3225–3233.

34 H. Shanks, C. J. Fang, L. Ley, M. Cardona, F. J. Demond and S. Kalbitzer, *Phys. Status Solidi B* 1980, **100**, 43–56.

Physical Chemistry Chemical Physics Accepted Manuscript

A table of contents entry:

This should include:

* Colour graphic: maximum size 8 cm x 4 cm
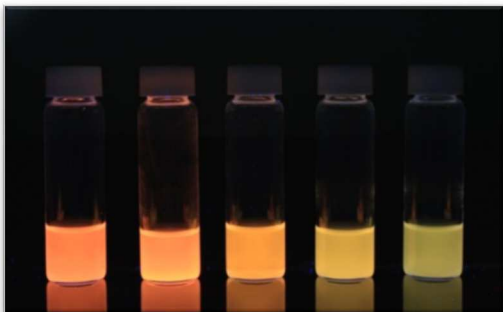
* Text: one sentence, of maximum 20 words, highlighting the novelty of the work:

A novel approach for producing and tuning the emission of a colloidal dispersion of amorphous porous silicon nanoparticles via controlled oxidation and disorder increase .